Supporting Information for

Photocatalytic generation of H_2O_2 over Z-scheme Fe_2O_3@C@1T/2H-MoS_2 heterostructured catalyst for high-performance Fenton reaction

Yang Yang,[a] Qianqian Wang,[a] Xueyong Zhang[b], Xianhe Deng,[c] Yina Guan,[c] Maoquan Wu,[a] Li Liu,[a] Jie Wu,[c] Tongjie Yao,[*a,b] Yadong Yin,[*b]

[a]*State Key Lab Urban Water Resource and Environment, School of Chemistry and Chemical Engineering, Harbin Institute of Technology, Harbin, China*
[b]*Department of Chemistry, University of California, Riverside, CA 92521 USA*
[c]*Key Laboratory of Functional Inorganic Material Chemistry, Ministry of Education, School of Chemistry and Materials Science, Heilongjiang University, Harbin, China*

Number of Pages: 22

Number of Figures: 14

Number of Tables: 3

Corresponding authors E-mail:yaotj@hit.edu.cn; yadong.yin@ucr.edu

Table of Contents

Supplementary Figures

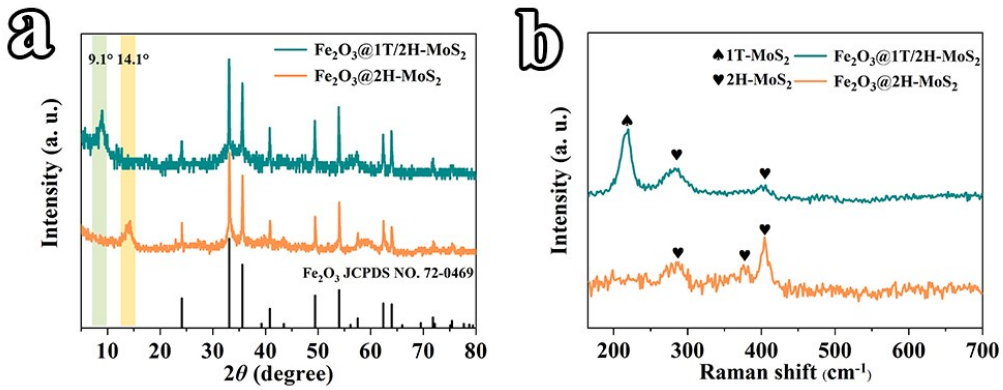

Fig. S1. (a) XRD and (b) Raman spectra of Fe_2O_3@2H-MoS_2 and Fe_2O_3@1T/2H-MoS_2. After calcination, the 1T-MoS_2 transferred to 2H-MoS_2.

The XRD pattern of Fe_2O_3@1T/2H-MoS_2 is shown in Fig. S1a. Besides the characteristic peaks of Fe_2O_3, the peak located at 9.1° corresponds to the (002) facet of 1T-MoS_2. In the Raman spectrum of Fe_2O_3@1T/2H-MoS_2 (Fig. S1b), three peaks appear at 226.4, 284.7, and 406.9 cm^{-1}, clearly indicating the mixed 1T- and 2H-phase in the as-prepared sample. After calcination, the peak at 226.4 cm^{-1} disappear, while one peak at 381.9 cm^{-1} is observed, suggesting the conversion of 1T-phase to 2H-phase. The phase transition of MoS_2 can be further verified by XRD patterns. After calcination, the (002) peak shifts from 9.1° to 14.4° assigned to the (002) facet of 2H-MoS_2.

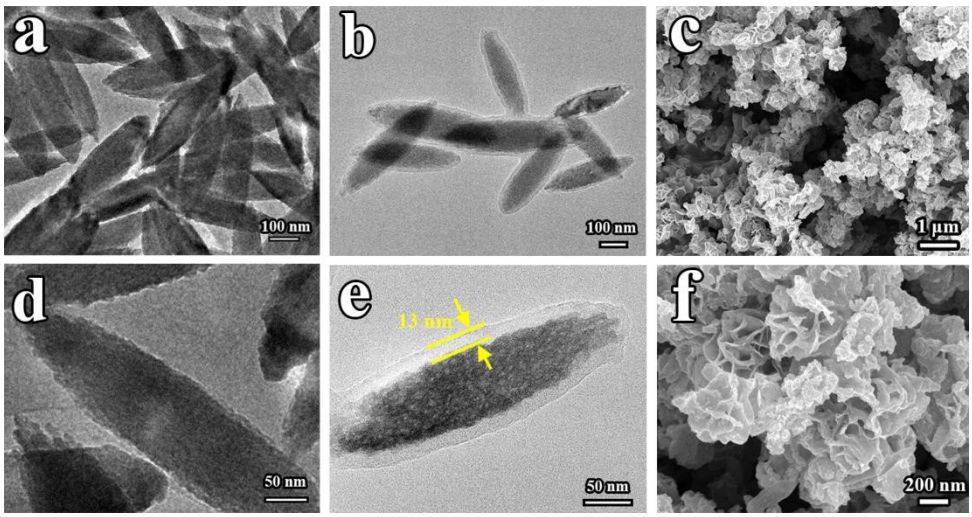

Fig. S2. TEM images of (a,d) Fe_2O_3 and (b,e) Fe_2O_3@C. (c,f) SEM images of Fe_2O_3@C@1T/2H-MoS_2.

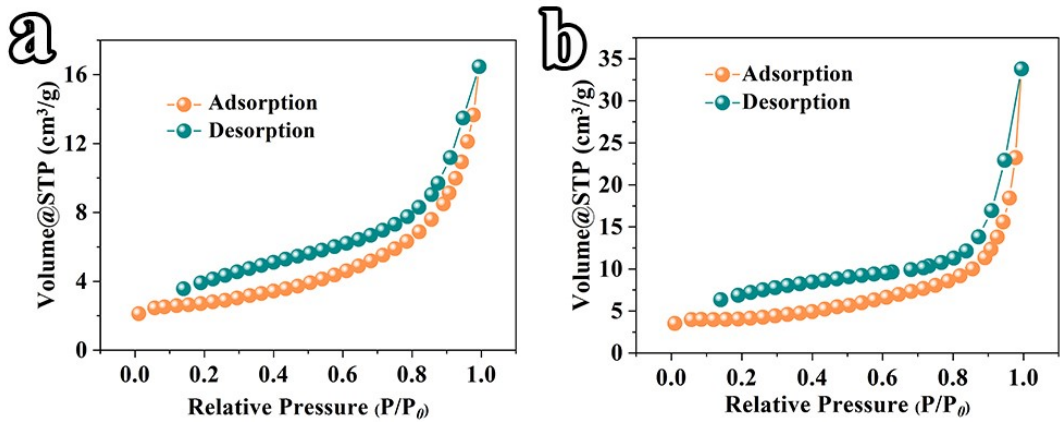

Fig. S3. Nitrogen adsorption-desorption isotherms of (a) Fe_2O_3@C and (b) Fe_2O_3@C@1T/2H-MoS_2.

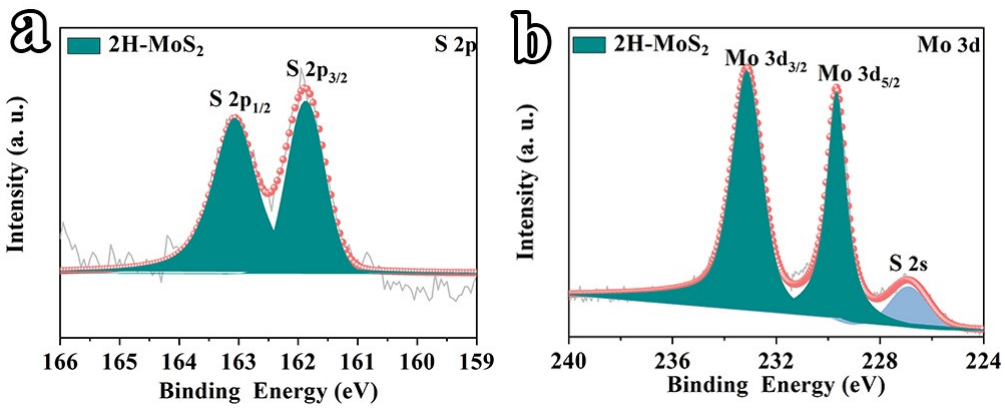

Fig. S4. XPS spectrum of Fe_2O_3@C@2H-MoS_2: (a) core-level spectrum of S 2p, and (b) core-level spectrum of Mo 3d.

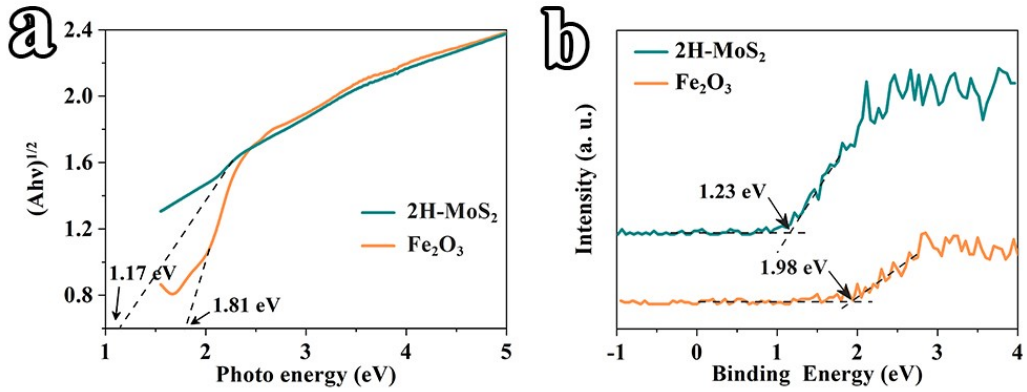

Fig. S5. (a) The plots of $(\alpha hv)^2$ *vs. hv* in Fe_2O_3 and 2H-MoS_2. (b) VB-XPS spectra of Fe_2O_3 and 2H-MoS_2.

$$(\alpha hv)^{1/n} = A(hv - E_g) \quad \text{(S1)}$$

$$E_{VB} = E_{CB} + E_g \quad \text{(S2)}$$

The bandgap energy (E_g) is determined using Tauc equation (Eq. S1, Fig. S5a), where α, h, v, A, and n is the absorption coefficient, Planck constant, frequency of light, a constant, and the transition property of the semiconductor (herein, n=1/2), respectively. E_g of Fe_2O_3 and 2H-MoS_2 is estimated to be 1.81 and 1.17 eV, respectively. According to the VB-XPS spectra (Fig. S5b), the VB position of Fe_2O_3 and 2H-MoS_2 locates at 1.98 and 1.23 eV, and the CB position is calculated to be 0.17 and 0.06 eV (Eq. S2), respectively.

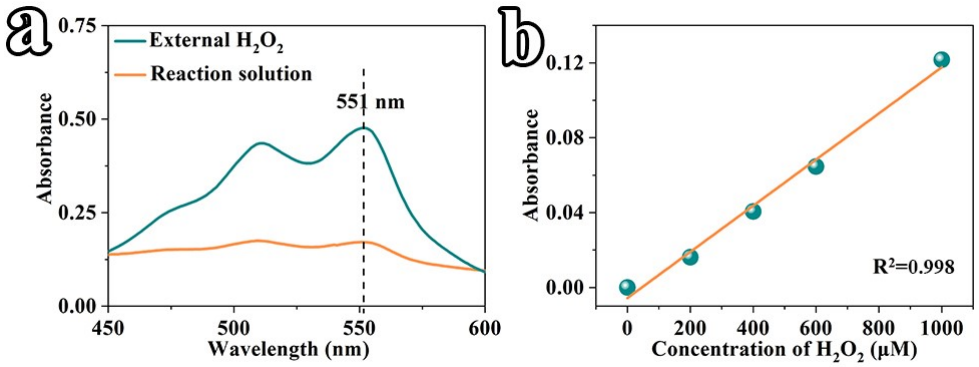

Fig. S6. (a) UV-vis spectra of H_2O_2 solution. (b) Relationship between absorbed intensity and H_2O_2 concentration.

In a DPD method, the relationship between the absorbed intensity and H_2O_2 concentration was calibrated according to the peak at 551 nm (Fig. S6a). In the range of 0-1000 μM, the correlation coefficient (R^2) was as high as 0.998, suggesting the work curve was reliable (Fig. S6b).

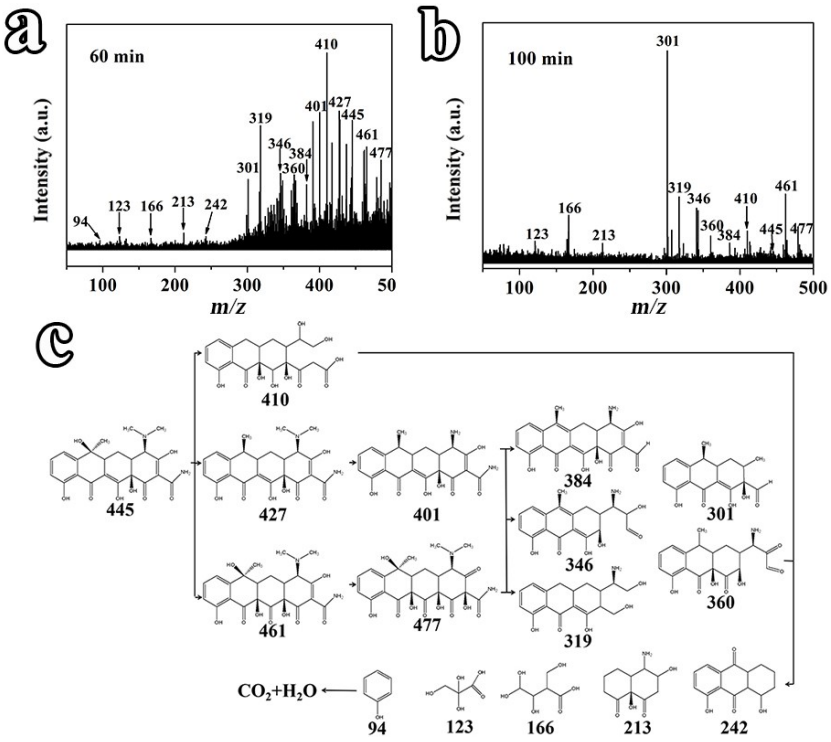

Fig. S7. Mass spectra of intermediates in the system of Fe_2O_3@C@1T/2H-MoS_2 after (a) 60 min and (b) 100 min. (c) Possible degradation pathway of TC in PSHFR catalyzed by Fe_2O_3@C@1T/2H-MoS_2.

The intermediate products of TC in the system of Fe_2O_3@C@1T/2H-MoS_2 were analyzed by HPLC-MS (Fig. S7). The signal of TC (*m/z*=445) is still detected after 60 min and almost disappears after 100 min (Figs. S7a-b). The possible degradation pathway of TC is shown in Fig. S7c. Under the attack of radicals, initial TC is oxidized to the compounds (*m/z*=410, 427, and 461) via dealkylation, dehydroxylation, and hydroxylation. An intermediate (*m/z*=401 or 477) is obtained via additional reaction between $^{\bullet}OH$ and TC, further evidencing $^{\bullet}OH$ is a main radical. Moreover, the signal of the characteristic intermediate (*m/z*=414) via reaction between TC and $^{\bullet}O_2^-$ is invisible, further verifying the minor contribution of $^{\bullet}O_2^-$. Next, the intermediates (*m/z*=401 and 477) undergo the dealkylation and hydroxylation

reactions, and the molecules with the lower molecule weight (*m/z*=384, 346, 319, 301, and 360) are produced. A ring-opening reaction directly occurs on the intermediate (*m/z*=410), and organics (*m/z*=242, 213, 166, 123, and 94) are formed and mineralized to CO_2 and H_2O.

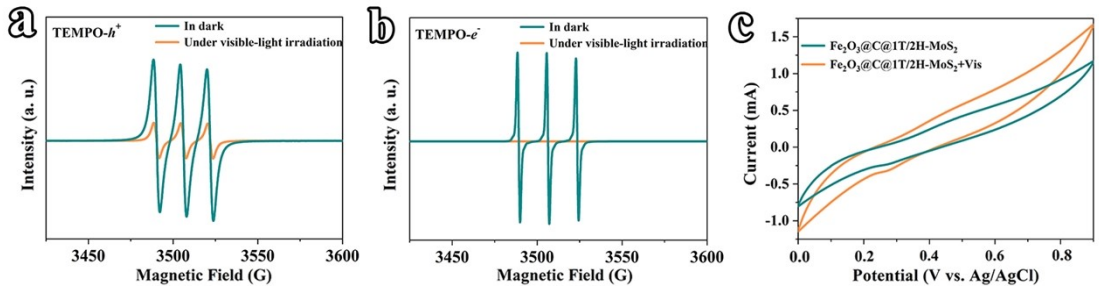

Fig. S8. ESR spectra for (a) TEMPO-h^+ and (b) TEMPO-e^-; (c) CV curves of Fe_2O_3@C@1T/2H-MoS_2 in dark or under visible light illumination.

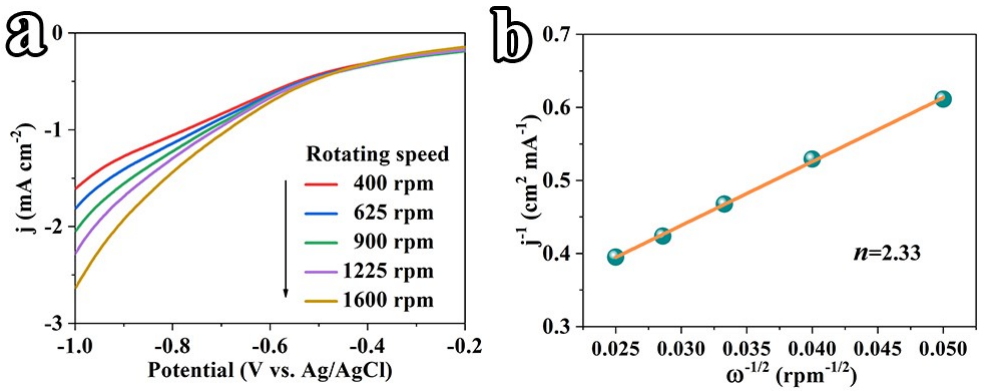

Fig. S9. (a) LSV curves of Fe_2O_3@C@1T/2H-MoS_2 under different rotating speeds; (b) Koutecky-Levich plots of the data obtained at the constant electrode potential (-1.0 V vs. Ag/AgCl).

$$j^{-1} = j_k^{-1} + B^{-1}\omega^{-1/2} \quad \text{(S3)}$$

$$B = 0.2nF\upsilon^{-1/6}CD^{2/3} \quad \text{(S4)}$$

In Fig. S9a, LSV curve of Fe_2O_3@C@1T/2H-MoS_2 is measured in an O_2-saturated phosphate buffer solution (0.1 mol L^{-1}) at different rotating speeds, and the corresponding Koutecky-Levich plots of the data at -1.0 V vs. Ag/AgCl is shown in Fig. S9b. The average number of electrons (n) involved in reduction of O_2 was obtained by the linear regression of the plots (Eqs. S3-S4), where j, j_k, ω, F, v, C, and D was the current density, the kinetic current density, the rotating speed, the Faraday constant (96,485 C mol^{-1}), the kinetic viscosity of water (0.01 cm^2 s^{-1}), the bulk concentration of O_2 in water (1.26×10^{-3} mol cm^{-3}), and the diffusion coefficient of O_2 (2.7×10^{-5} cm^2 s^{-1}), respectively.

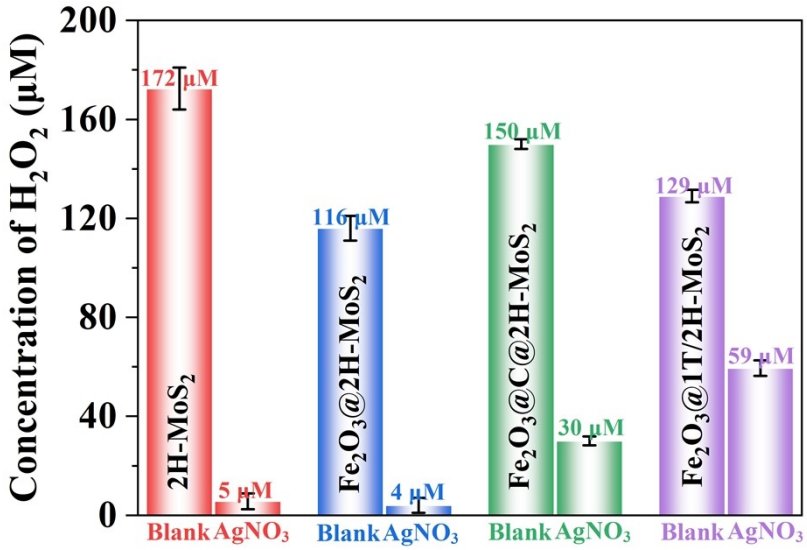

Fig. S10. H_2O_2 generation of different catalysts in the presence of $AgNO_3$.

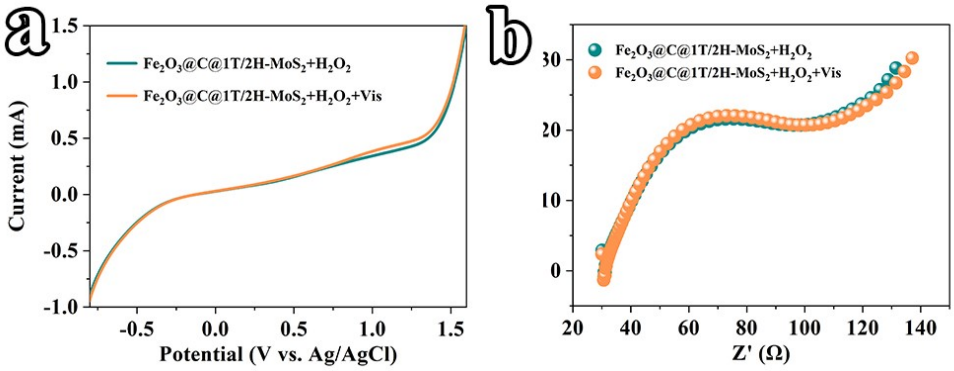

Fig. S11. (a) LSV and (b) EIS curves of Fe_2O_3@C@1T/2H-MoS_2 under different conditions.

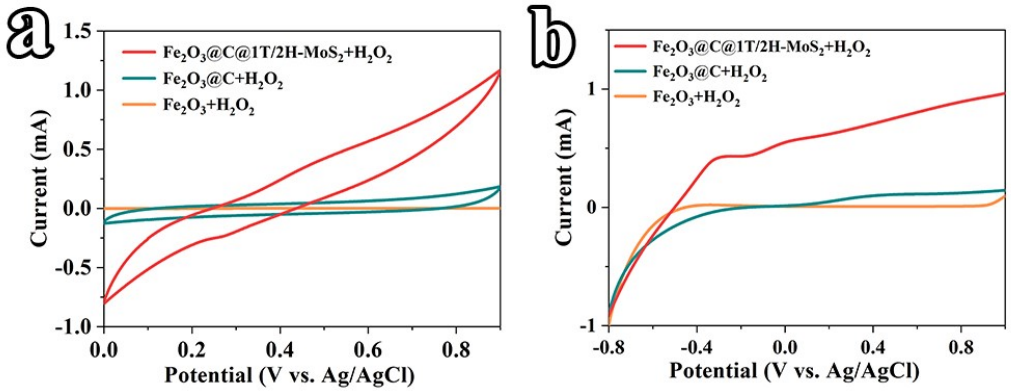

Fig. S12. (a) CV and (b) LSV curves of different catalysts with external H_2O_2.

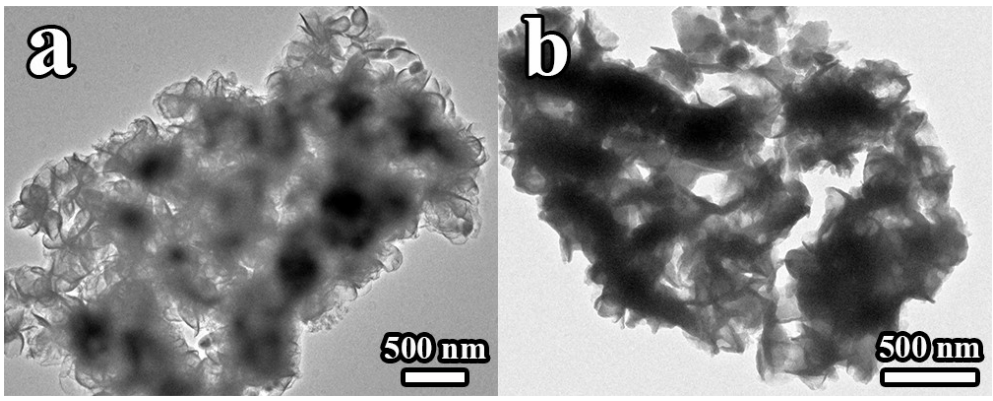

Fig. S13. TEM images of (a) fresh Fe_2O_3@C@1T/2H-MoS_2 and (b) recycled Fe_2O_3@C@1T/2H-MoS_2.

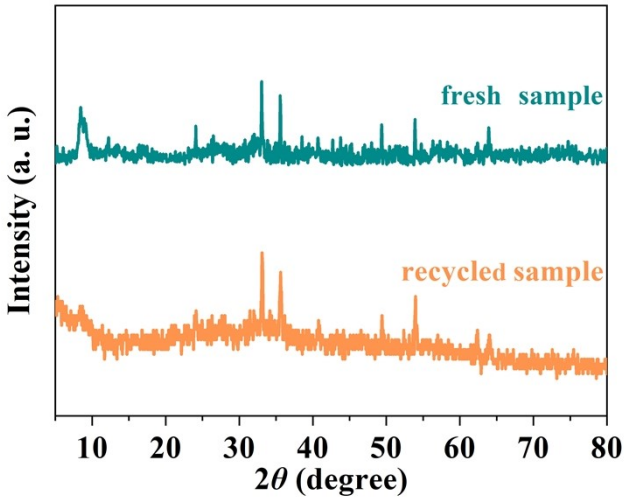

Fig. S14. XRD patterns of Fe_2O_3@C@1T/2H-MoS_2 before and after reaction.

Supplementary Tables

Table S1. Comparison of production rate of H_2O_2 with other works.

Catalysts[a]	Catalyst dosage (g/L)	Atmosphere	Reaction solution[b]	Light source	pH	H_2O_2 production activity (μmol/g/h)	Ref.
Fe_2O_3@MoS_2@Ag	1.0	Air	Water (50 mL)	Vis	/	95	[1]
Au@MoS_2	1.0	Air	Water (50 mL)	Vis	5.0	54	[2]
N-defective g-C_3N_4	1.0	Air	Water (20 mL)	Vis	3.0	211	[3]
g-C_3N_4@MoS_2	0.4	Air	Water (50 mL)	UV–Vis	/	300	[4]
O/K-CN	0.5	O_2-saturated	10 vol% IPA (50 mL)	Vis	/	1547	[5]
Ag@U-g-C_3N_4-NS	1.0	O_2-saturated	Water (100 mL)	Vis	3.0	45	[6]
1T-MoS_2/g-C_3N_4	0.1	Air	IPA (50 mL)	UV–Vis	7.0	440	[7]
SCN	0.5	Air	10 vol% IPA (40 mL)	Vis	5.8	28	[8]
Ultrathin g-C_3N_4	1.0	O_2-saturated	5 vol% EtOH (50 mL)	UV–Vis	/	1083	[9]
Ti_3C_2@g-C_3N_4	1.0	O_2-saturated	10 vol% IPA (50 mL)	Vis	/	132	[10]
g-C_3N_4	0.5	O_2-saturated	10 vol% IPA (100 mL)	Vis	/	574	[11]
OCN	1.0	O_2-saturated	10 vol% IPA (100 mL)	Vis	7.0	1200	[12]
Ag_3PO_4@$NiFe_2O_4$	0.3	Air	75 vol% MeOH (50 mL)	Vis	/	150	[13]
Ni-CAT-CN_{60}	0.7	Air	Water (15 mL)	Vis	/	1801	[14]
Cv@g-C_3N_4	1.0	O_2-saturated	10 vol% EtOH (10 mL)	Vis	/	7.0	[15]
Fe_2O_3@C@1T/2H-MoS_2	0.2	Air	75 vol% MeOH (50 mL)	Vis	6.5	1575	here

[a]O/K-CN = oxygen and potassium dual-heteroatom incorporated polymeric carbon nitride, U-g-C_3N_4-NS = ultrathin g-C_3N_4 nanosheets, SN-GQD = sulfur and nitrogen co-doped graphene quantum dots, SCN = SnO_2-coupled and cyano modified g-C_3N_4, OCN = oxygen-enriched graphitic carbon nitride polymers, Ni-CAT-CN_{60} = C_3N_4 assisted $Ni_3(HHTP)_2$, Cv = cyano group; [b]IPA = isopropanol, EtOH = ethanol.

Table S2. Comparison of the degradation performance with other works.

Catalysts[a]	Catalyst dosage (g/L)	Light source	Pollutants[b]	pH	Amount	Removal time	Ref.
$Fe_2O_3/MoS_2/Ag$	1.0	Vis	2,4-DCP	5.0	30 mL, 10 mg L^{-1}	150 min (99.0%)	[1]
Fe_2O_3/MoS_2	0.3	UV-Vis	MB	4.0	30 mL, 20 mg L^{-1}	20 min (97.0%)	[16]
RGO-Fe_2O_3-MoS_2	0.1	Vis	MB	/	50 mL, 10 mg L^{-1}	50 min (98.0%)	[17]
Fe_2O_3/ACN	0.5	UV-Vis	OTC	9.0	100 mL, 30 mg L^{-1}	120 min (92.6%)	[18]
Fe_2O_3@PPy/PB	0.2	Vis	TC	6.5	50 mL, 50 mg L^{-1}	35 min (21.3%)	[19]
Fe_2O_3/CeO_2	0.06	Vis	TC	13.0	50 mL, 30 mg L^{-1}	60 min (88.6%)	[20]
rGO/Fe_2O_3/g-C_3N_4	1.0	Vis	TC	7.0	100 mL, 50 mg L^{-1}	40 min (≈98.0%)	[21]
$BiVO_4$/α-Fe_2O_3	0.5	Vis	TC	/	100 mL, 20 mg L^{-1}	120 min (75.8%)	[22]
g-C_3N_4/MoS_2/graphene	0.3	Vis	TC	/	60 mL, 1.0 mg L^{-1}	60 min (69.0%)	[23]
$MoS_2/ZnSnO_3$	0.5	Vis	TC	/	50 mL, 30 mg L^{-1}	60 min (80.2%)	[24]
$NiSe_2/MoS_2$	0.6	Solar	TC	/	50 mL, 20 mg L^{-1}	120 min (58.1%)	[25]
$MnFe_2O_4$-Au	0.1	Vis	TC	6.0	100 mL, 20 mg L^{-1}	90 min (88.3%)	[26]
Fe_2O_3@C@1T/2H-MoS_2	0.2	Vis	TC	6.5	50 mL, 100 mg L^{-1}	100 min (91.5%)	here

[a]RGO = reduced graphene oxide, ACN = cyclized carbon nitride, PPy = polypyrrole, PB = Prussian blue; [b]MB = methyl blue, 2,4-DCP = 2,4-dichlorophenol, RhB = Rhodamine B, OTC = oxytetracycline.

Table S3. Fe^{2+} content of different catalysts before and after Fenton reaction. The amount of external H_2O_2 was equal to the yield over Fe_2O_3@C@1T/2H-MoS_2 within 100 min.

Catalysts	Fresh sample	Recycled sample
Fe_2O_3	7.0%	3.1%
Fe_2O_3@C	21.2%	24.0%
Fe_2O_3@C@1T/2H-MoS_2	23.0%	27.8%

References in Supporting Information

[1] M. J. Guo, Z. P. Xing, T. Y. Zhao, Y. L. Qiu, B. Tao, Z. Z. Li, W. Zhou, *Appl. Catal. B: Environ.* **2020**, *272*, 118978.

[2] H. Y. Song, L. S. Wei, C. X. Chen, C. C. Wen, F. Q. Han, *J. Catal*. **2019,** *376*, 198-208.

[3] X. Zhang, P. J. Ma, C. Wang, L. Y. Gan, X. J. Chen, P. Zhang, Y. Wang, H. Li, L. H. Wang, X. Y. Zhou, K. Zheng, *Energy Environ. Sci.* **2022***, 15, 830*.

[4] L. Z. Qin, Y. Z. Lin, Y. C. Dou, Y. J. Yang, K. Li, T. Li, F. T. Liu, *Nanoscale* **2020**, *12*, 13829.

[5] W. Liu, P. F. Wang, J. Chen, X. Gao, H. N. Che, B. Liu, Y. H. Ao, *Adv. Funct. Mater*. **2022**, 2205119.

[6] J. S. Cai, J. Y. Huang, S. C. Wang, J. Iocozzia, Z. T. Sun, J. Y. Sun, Y. K. Yang, Y. K. Lai, Z. Q. Lin, *Adv. Mater*. **2019**, *31*, 1806314.

[7] X. Y. Hu, X. K. Zeng, Y. Liu, J. Lu, S. Yuan, Y. C. Yin, J. Hu, D. T. McCarthy, X. W. Zhang, *Appl. Catal. B: Environ.* **2020**, *268*, 118466.

[8] C. C. Chu, W. Miao, Q. J. Li, D. D. Wang, Y. Liu, S. Mao, *Chem. Eng. J.* **2022***, 428,* 132531.

[9] L. Zhou, J. R. Feng, B. C. Qiu, Y. Zhou, J. Y. Lei, M. Y. Xing, L. Z. Wang, Y. B. Zhou, Y. D. Liu, J. L. Zhang, *Appl. Catal. B: Environ.* **2020**, *267*, 118396.

[10] Y. Yang, Z. T. Zeng, G. M. Zeng, D. L. Huang, R. Xiao, C. Zhang, C. Y. Zhou, W. P. Xiong, W. J. Wang, M. Cheng, W. J. Xue, H. Guo, X. Tang, D. H. He, *Appl. Catal. B: Environ.* **2019**, *258*, 117956.

[11] C. Y. Feng, L. Tang, Y. C. Deng, J. J. Wang, J. Luo, Y. N. Liu, X. L. Ouyang, H. R. Yang, J. F. Yu, J. J. Wang, *Adv. Funct. Mater*. **2020**, 2001922.

[12] Z. Wei, M. L. Liu, Z. J. Zhang, W. Q. Yao, H. W. Tan, Y. F. Zhu, *Energy Environ. Sci*. **2018**, *11*, 2581.

[13] S. Q. Huang, Y. G. Xu, T. Zhou, M. Xie, Y. Ma, Q. Q. Liu, L. Q. Jing, H. Xu, H. M. Li, *Appl. Catal. B: Environ.* **2018**, *225*, 40-50.

[14] Y. J. Zhao, Y. Liu, Z. Z. Wang, Y. R. Ma, Y. J. Zhou, X. F. Shi, Q. Y. Wu, X. Wang, M. W. Shao, H. Huang, Y. Liu, Z. H. Kang, *Appl. Catal. B: Environ.* **2021**, *289*, 120035.

[15] L. Chen, C. Chen, Z. Yang, S. Li, C. H. Chu, B. L. Chen, *Adv. Funct. Mater.* **2021***, 31,* 2105731.

[16] S. Wang, B. W. Tang, W. L. Yang, F. M. Wu, G. Y. Zhang, B. Zhao, X. J. He, Y. Q. Yang, J. X. Jiang, *J. Alloy. Compd*. **2019**, *784*, 1099-1105.

[17] L. X. Chen, F. He, N. Q. Zhao, R. S. Guo, L. X. Chen, F. He, N. Q. Zhao, R. S. Guo, *Appl. Surf. Sci.* **2017**, *420,* 669-680.

[18] Y. P. Li, J. Han, K. L. Liu, J. H. Li, H. X. Zhang, J. X. Chen, *Sep. Purif. Technol.* **2022**, *290*, 120790.

[19] Y. Yang, S. C. Ma, J. P. Qu, J. Q. Li, Y. Liu, Q. Q. Wang, J. Jing, Y. Yuan, T. J. Yao, J. Wu, *J. Hazard. Mater.* **2021**, *405*, 124668.

[20] S. He, C. Yan, X. Z. Chen, Z. Wang, T. Ouyang, M. L. Guo, Z. Q. Liu, *Appl. Catal. B: Environ.* **2020**, *276,* 119138.

[21] S. Shanavas, S. M. Roopan, A. Priyadharsan, D. Devipriya, S. Jayapandi, R. Acevedo, P. M. Anbarasan, *Appl. Catal. B: Environ.* **2019**, *255*, 117758.
[22] C. C. Ma, J. Lee, Y. Kim, W. C. Seo, H. Jung, W. Yang, *J. Colloid Interf. Sci.* **2021**, *581*, 514522.
[23] H. W. Tian, M. Liu, W. T. Zheng, *Appl. Catal. B: Environ.* **2018**, *225*, 468-476.
[24] F. Guo, X. L. Huang, Z. H. Chen, H. J. Ren, M. Y. Li, L. Z. Chen, *J. Hazard. Mater.* **2020**, *390*, 122158.
[25] J. Jia, L. S. Zheng, K. K. Li, Y. T. Zhang, H. J. Xie, *Chem. Eng. J.* **2022**, *429*, 132432.
[26] L. Qin, Z. H. Wang, Y. K. Fu, C. Lai, X. G. Liu, B. S. Li, S. Y. Liu, H. Yi, L. Li, M. M. Zhang, Z. W. Li, W. C. Cao, Q. Y. Niu, *J. Hazard. Mater.* **2021**, *414*, 125448.